Crystal Structure of Nucleotide-Free Diphtheria Toxin[†,‡]

Charles E. Bell and David Eisenberg*

UCLA-DOE Laboratory of Structural Biology and Molecular Medicine, Molecular Biology Institute, and Department of Chemistry and Biochemistry, Box 951569, University of California at Los Angeles, Los Angeles, California 90095-1569

ABSTRACT: The crystal structure of diphtheria toxin (DT) in the absence of nucleotide (nucleotide-free DT) has been determined at 2.3 Å resolution to a crystallographic *R* factor and free *R* factor of 18.2 and 28.2%, respectively. A comparison of this structure to the previously determined structures of DT in complex with adenylyl(3′-5′)uridine monophosphate (ApUp) and DT in complex with nicotinamide adenine dinucleotide (NAD) reveals that there are no significant movements of the two subdomains of the catalytic (C) domain associated with dinucleotide binding. The side chains of six residues within the active-site cleft, including Tyr65, Pro38, Tyr27, Thr23, Glu148, and Tyr54, show movements of up to 3 Å upon dinucleotide binding. In the structure of nucleotide-free DT, the active-site loop residues 39−47 of the C domain are well ordered and extend over the active-site cleft in approximately the same position as in the structure of DT in complex with ApUp. This is in contrast to the structure of the DT−NAD complex, in which the active-site loop is disordered. On the basis of a comparison of the nucleotide-free and NAD-bound DT structures, we suggest that the interaction of NAD with Pro38 and also possibly Tyr54 and Trp153 could disrupt the network of hydrogen bonds that stabilizes the position of the active-site loop over the active-site cleft, allowing this loop to become disordered. This may be an important step in binding of the C domain of DT to its substrate, elongation factor-2.

A wide variety of ADP ribosyltransferase (ADP-RT[1]) enzymes, in both eukaryotes and prokaryotes, catalyze the transfer of an ADP ribose group from NAD to a specific residue within a specific protein substrate, altering the protein's activity. Among these enzymes are several bacterially secreted toxins, including diphtheria toxin (DT), cholera toxin (CT), *Escherichia coli* heat-labile enterotoxins (LT-I and LT-IIb), *Pseudomonas aeruginosa* exotoxin A (ETA), pertussis toxin (PT), and several clostridial toxins. Each of these toxins catalyzes the ADP ribosylation of a specific host protein, resulting in a detrimental effect on the host (Passador & Iglewski, 1994; Burnette, 1994; Moss & Vaughn, 1990).

DT was the first toxin discovered to act by ADP ribosylation (Collier, 1975; Pappenheimer, 1977) and has since been one of the most extensively characterized proteins with ADP-RT activity. DT is a 58 kDa, 535-residue protein (Greenfield et al., 1983) secreted by strains of *Corynebacterium diphtheriae* which have been infected by a phage carrying the DT gene (Freeman, 1951). In humans, DT causes the disease diphtheria by killing host cells. DT consists of a C-terminal receptor-binding (R) domain (residues 385−535), a central translocation (T) domain (residues 201−384), and an N-terminal catalytic (C) domain (residues 1−191). While the R and T domains facilitate delivery of the C domain to the cytoplasm of a host cell, the C domain shuts down protein synthesis within the cell by catalyzing the ADP ribosylation of elongation factor-2 (EF-2) at diphthamide, a modified histidine residue (van Ness et al., 1980).

The structures of monomeric and dimeric forms of DT, and of the isolated C domain, have been determined to atomic resolution by X-ray crystallography (Choe et al., 1992; Bennett et al., 1994; Bennett & Eisenberg, 1994; Weiss et al., 1995). Each of these crystal structures of DT was determined in complex with the dinucleotide adenylyl(3′-5′)uridine monophosphate (ApUp), which is an inhibitor of the ADP ribosylation reaction. Recently, the crystal structure of dimeric DT bound to NAD was also determined (Bell & Eisenberg, 1996). Both ApUp and NAD bind to a cleft in the C domain formed at the interface of two subdomains (Figure 1). Each subdomain consists of a mostly antiparallel β-sheet of three or five strands surrounded by three or four α-helices. The two β-sheets meet at roughly a right angle, forming the subdomain interface. A homologous fold is shared by the catalytic domains of all other ADP-ribosylating toxins whose structures have been determined, including PT (Stein et al., 1994), LT-I (Sixma et al., 1993), LT-IIb (van den Akker et al., 1996), CT (Zhang et al., 1995), and ETA (Allured et al., 1986). Limited but significant sequence homology suggests that this fold is shared by other ADP ribosylating bacterial toxins and also by mammalian enzymes with ADP-ribosylation activity (Takada et al., 1995). Indeed, the catalytic fragment of poly(ADP ribose) polymerase from

[1] Abbreviations: DT, diphtheria toxin; C domain, catalytic domain of DT; T domain, translocation domain of DT; R domain, receptor-binding domain of DT; NAD, nicotinamide adenine dinucleotide; ApUp, adenylyl(3′−5′)uridine monophosphate; ADP-RT, adenosine 5′-diphosphate ribosyltransferase; dDT-nf, nucleotide-free dimeric DT; dDT−NAD, dimeric DT in complex with NAD; dDT−ApUp, dimeric DT in complex with ApUp; NMN, nicotinamide mononucleotide portion of NAD; EF-2, elongation factor-2; ETA, *Pseudomonas aeruginosa* exotoxin A; PT, pertussis toxin; LT-I, *Escherichia coli* type I heat-labile enterotoxin; LT-IIb, *E. coli* type IIb heat-labile enterotoxin; CT, cholera toxin of *Vibrio cholerae*; rms, root-mean-square; PDB, Brookhaven Protein Data Bank; PEG, polyethylene glycol.
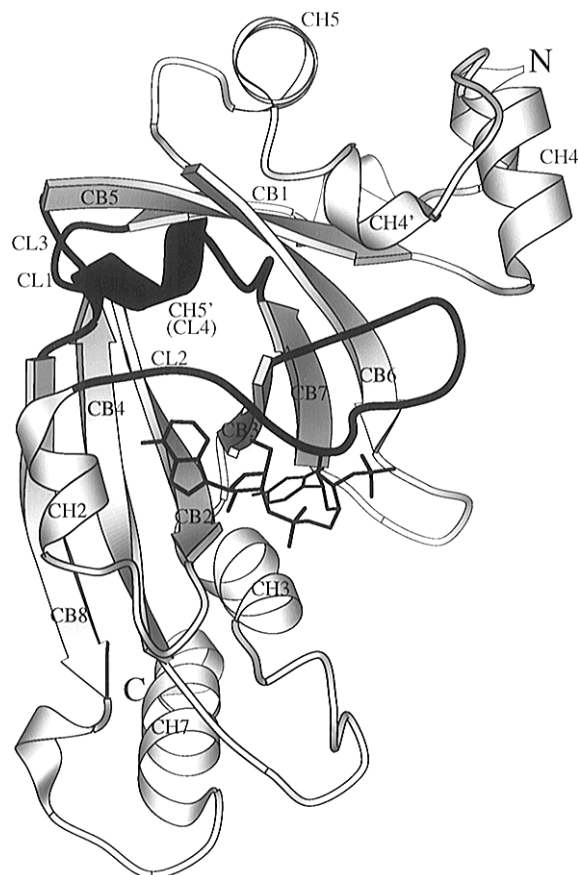
© 1997 American Chemical Society

FIGURE 1: Ribbon drawing of the catalytic (C) domain of DT bound to ApUp (PDB entry 1DDT; Bennett et al., 1994). α-Helices are labeled CH2–CH7, and β-strands are labeled CB1–CB8, according to Bennett et al. (1994). ApUp, shown in black lines, binds to a cleft formed at the interface of two subdomains. The upper subdomain is formed by CB3, CB7, CB6, CB5, CB1, CH4, CH4′, and CH5. The lower subdomain is formed by CB8, CB4, CB2, CH2, CH3, and CH7. The two subdomains are connected by four "hinge-loops" (CL1–CL4) shown in black. The central part of CL4 was shown to form a short α-helix in the 2.0 Å refined structure of dDT–ApUp (Bennett et al., 1994) and is shown as such. Notice that the active-site loop (CL2), residues 34–52, extends over the active-site cleft, making contacts with ApUp. This figure and Figures 2 and 3 were prepared using MOLSCRIPT (Kraulis, 1991).

chicken was recently shown to posses a fold related to the ADP-ribosylating toxins (Ruf et al., 1996).

In the structure of the C domain of DT, the connections between the two subdomains are formed by several "hinge-loops" CL1–CL4 (Choe et al., 1992). These hinge-loops appear to endow the C domain with the potential for flexibility. While in the structures of DT bound to NAD and ApUp there are no significant differences in the positions of the two subdomains relative to one another, it is possible that nucleotide binding could be accompanied by rotation of the two subdomains relative to one another, resulting in formation of the active-site cleft. However, since the structure of the nucleotide-free state of DT has not been previously determined, the possibility of such movements has remained in question.

Residues 34–52 of the C domain form a long extended loop (CL2 in Figure 1) over the nucleotide-binding site which has been termed the "active-site" loop. In all of the structures of DT bound to ApUp, this loop is well ordered and forms contacts with ApUp. These contacts appear to stabilize the position of the active-site loop over the active-site cleft. Thus,

it was postulated that the active-site loop may be disordered in the nucleotide-free state and may clamp down to form interactions with NAD similar to those observed for ApUp (Bennett et al., 1994). Surprisingly, however, in the structure of DT bound to NAD, residues 39–47 of the active-site loop were not observed in electron density maps (for each of two copies of DT in the asymmetric unit of the crystal) and were assumed to be disordered. Since the active-site loop is evidently not involved in NAD binding, it was suggested that this loop of the C domain could potentially be important for binding to the ADP ribose acceptor substrate, EF-2 (Bell & Eisenberg, 1996). Because the active-site loop is ordered in the DT–ApUp complex, and disordered in the DT–NAD complex, an important question has emerged. Does ApUp binding stabilize this loop, or does NAD binding destabilize this loop? In other words, what is the conformation of the active-site loop in the nucleotide-free state?

In order to (1) determine if there are movements of the two subdomains relative to one another upon nucleotide binding and (2) clearly define the position of the active-site loop in the absence of nucleotide as compared to that of the NAD- and ApUp-bound forms, we have determined the structure of the nucleotide-free form of DT at 2.3 Å resolution.

MATERIALS AND METHODS

DT Purification and Crystallization. Partially purified, unnicked DT was purchased from Connaught Laboratories (Willowdale, Ontario, Canada) and further purified as has been described (Carroll et al., 1986). A chromatographic step on DyeMatrex Gel Green A was added in order to separate the nucleotide-free from the nucleotide-bound DT fractions. Subsequently, a 280/260 nm absorbance ratio was measured and found to be 1.7. This verifies that the purified DT is indeed nucleotide-free, whereas lower values would indicate the presence of nucleotides such as ApUp (Carroll et al., 1986). Nucleotide-free dimeric DT was crystallized using the hanging drop vapor diffusion method in which the reservoir consisted of 12% (w/v) polyethylene glycol (PEG) 8000, 0.43 M NaCl, and 0.043 M Tris buffer (pH 7.5), and the hanging drop was prepared by mixing 2 μL of 25 mg/mL DT and 8 μL of 14% (w/v) PEG 8000, 0.5 M NaCl, and 0.05 M Tris buffer (pH 7.5).

X-ray Data Collection. A crystal was prepared for data collection by removing it from the original mother liquor and soaking in cryoprotectant solution containing 18% (w/v) PEG 8000, 0.5 M NaCl, 0.05 M Tris (pH 7.5), and 20% glycerol for approximately 10 min. The crystal was then mounted in a hair loop and flash-frozen at −180 °C under nitrogen vapor cooled by liquid nitrogen. During data collection, the crystal was maintained at −180 °C under the nitrogen vapor stream. The X-ray reflection intensities were measured with a Rigaku R-Axis IIC imaging plate using a Rigaku RU-200 X-ray generator operating at 50 kV and 100 mA, equipped with a copper anode (λ = 1.54 Å) and Molecular Structure Corp. double-focusing mirrors. The X-ray reflection intensities were integrated, merged, and scaled using the R-Axis II data-processing software package. Unit cell dimensions and data collection parameters are shown in Tables 1 and 2, respectively.

Crystallographic Refinement. Since the nucleotide-free dimeric DT crystal is nearly isomorphous with respect to

Table 1: Unit Cell Dimensions of Nucleotide-Free, ApUp-Bound, and NAD-Bound Crystal Forms of Dimeric DT[a]

	nucleotide-free dDT	dDT−ApUp[b]	dDT−NAD[c]
space group	C2	C2	C2
a (Å)	105.2	105.6	105.0
b (Å)	91.2	91.6	89.5
c (Å)	65.3	65.6	130.1
β (deg)	94.2	94.6	94.0
no. of DT/au[d]	1	1	2

[a] Crystals of all three forms were soaked in cryoprotectant containing 18% (w/v) PEG 8000, 0.5 M NaCl, 0.05 M Tris buffer (pH 7.5), and 20% (v/v) glycerol and subsequently flash-frozen at −180 °C. [b] From Bennett et al. (1994). [c] From Bell and Eisenberg (1996). [d] Number of DT molecules (monomers) per asymmetric unit of the crystal.

Table 2: X-ray Intensity Measurements for Nucleotide-Free Dimeric DT

no. of crystals	1
resolution (Å)	2.3
no. of observations	74 281
no. of unique reflections	26 627
completeness (%)	95.7 (92.7)[a]
R_{sym}[b] (%)	6.6 (23.9)
$\langle I/\sigma \rangle$	9.6 (2.6)
B overall[c] (Å²)	33.9

[a] Numbers in parentheses refer to the 2.3−2.4 Å resolution data only. [b] $R_{sym} = 100\sum_h |I_h - \langle I \rangle|/\sum_h I_h$. [c] Overall temperature factor as estimated from a Wilson plot using data from 3.0 to 2.3 Å.

Table 3: Refinement Statistics for Nucleotide-Free Dimeric DT

resolution limits (Å)	8.0−2.3
no. of reflections in working set	23 161
no. of reflections in test set (10%)	2565
final R factor[a] (%)	18.2
final free R factor[b] (%)	28.2
no. of atoms (non-hydrogen)	
protein	4021
water	358
rms deviations from ideal geometry	
bonds (Å)	0.01
angles (deg)	1.5
dihedrals (deg)	24.3
impropers (deg)	1.4
mean temperature factors (Å²)	
all atoms	38.8
protein	38.6
water	38.8

[a] $R = 100\sum_h ||F_o| - |F_c||/\sum_h |F_o|$. [b] The free R factor was calculated for 10% of the data which were omitted from the refinement.

Table 4: Structural Alignment of dDT-nf with dDT−ApUp and dDT−NAD[a]

	dDT−ApUp	dDT−NAD1	dDT−NAD2[b]
dDT-nf	0.26 (0.22)[c]	0.44 (0.30)	0.44 (0.29)

[a] Each entry gives the rms deviation in atomic positions (angstroms) between the two aligned structures. All alignments were done using Cα atoms only and the algorithm of Kabsch (1978). [b] For dDT−NAD, there are two molecules in the asymmetric unit of the crystal. [c] Numbers in parentheses refer to alignments of the C domains only.

the dimeric DT−ApUp crystal (see Table 1), the refinement of the nucleotide-free dimeric DT structure began with the refined dimeric DT−ApUp model (PDB entry 1DDT; Bennett et al., 1994) after removal of the ApUp. This starting model contained 4021 non-hydrogen protein atoms and 405 water molecules. Crystallographic refinement was performed using X-PLOR (Brünger, 1990). Prior to refinement, the R factor was 36.0%. After rigid body refinement, the R factor dropped to 26.8%. At this point, 10% of the reflections (2565) were sequestered into a test set in order to monitor the free R factor. After simulated annealing and restrained temperature factor refinement, the R factor and free R factor were 18.4 and 28.4%, respectively. Water molecules showing poor $2F_o - F_c$ density or temperature factors of >60 Å² were removed from the model, and additional waters were built into $F_o - F_c$ maps at peaks of >3σ. A second round of refinement was performed, resulting in a final model with an R factor and a free R factor of 18.2 and 28.2%, respectively. Refinement parameters are shown in Table 3. The atomic coordinates and structure factors have been deposited in the Brookhaven Protein Data Bank (PDB entry 1SGK).

RESULTS AND DISCUSSION

Overall Conformation of Nucleotide-Free DT. Crystals of nucleotide-free dimeric DT (dDT-nf) were grown using conditions similar to those used to obtain form IV crystals of dimeric DT in complex with ApUp (dDT−ApUp; Fujii et al., 1991), and crystals of dDT−nf and dDT−ApUp (Bennett et al., 1994) are nearly isomorphous (see Table 1). This was a preliminary indication that there are no major structural differences between dDT-nf and dDT−ApUp, such as domain or subdomain movements. After refinement of the dDT-nf structure, least-squares alignment with the structure of dDT−ApUp (Table 4 and Figure 2) confirms

that there are no significant differences in the positions of the R, T, and C domains or of the two subdomains of the C domain.

Crystals of dDT-nf, however, are not isomorphous with respect to crystals of dimeric DT bound to NAD (dDT−NAD), which were prepared by soaking dDT-nf crystals in an excess of NAD (Bell & Eisenberg, 1996). In fact, soaking the dDT-nf crystals in NAD led to a dramatic change in the unit cell dimensions (see Table 1), suggesting that significant structural changes occur upon NAD binding. However, an alignment of the refined dDT-nf structure with the dDT−NAD structure (Table 4 and Figure 2) indicates that there are no major differences between dDT-nf and dDT−NAD in either the positions of the individual domains of DT or the positions of the subdomains of the C domain. Rather, as discussed in detail below, the major structural changes induced by NAD binding which cause the change in unit cell dimensions are restricted to residues 39−47 of the active-site loop.

In summary, a comparison of the refined structure of dDT-nf with the structures of dDT−ApUp and dDT−NAD reveals that there are no significant movements of the two subdomains of the C domain relative to one another associated with nucleotide binding. Although the potential for flexibility is suggested by the structure of the C domain, in which two subdomains are connected by several hinge-loops (Choe et al., 1992), structures of the ApUp-bound, NAD-bound, and nucleotide-free forms of DT would suggest that the structure of the C domain is quite rigid. However, it is possible that movement of the two subdomains of the C domain relative to one another could occur upon binding to the ADP ribose acceptor substrate EF-2.

Movement of Specific Active-Site Residues. Minor differences in the positions of specific side chains within the
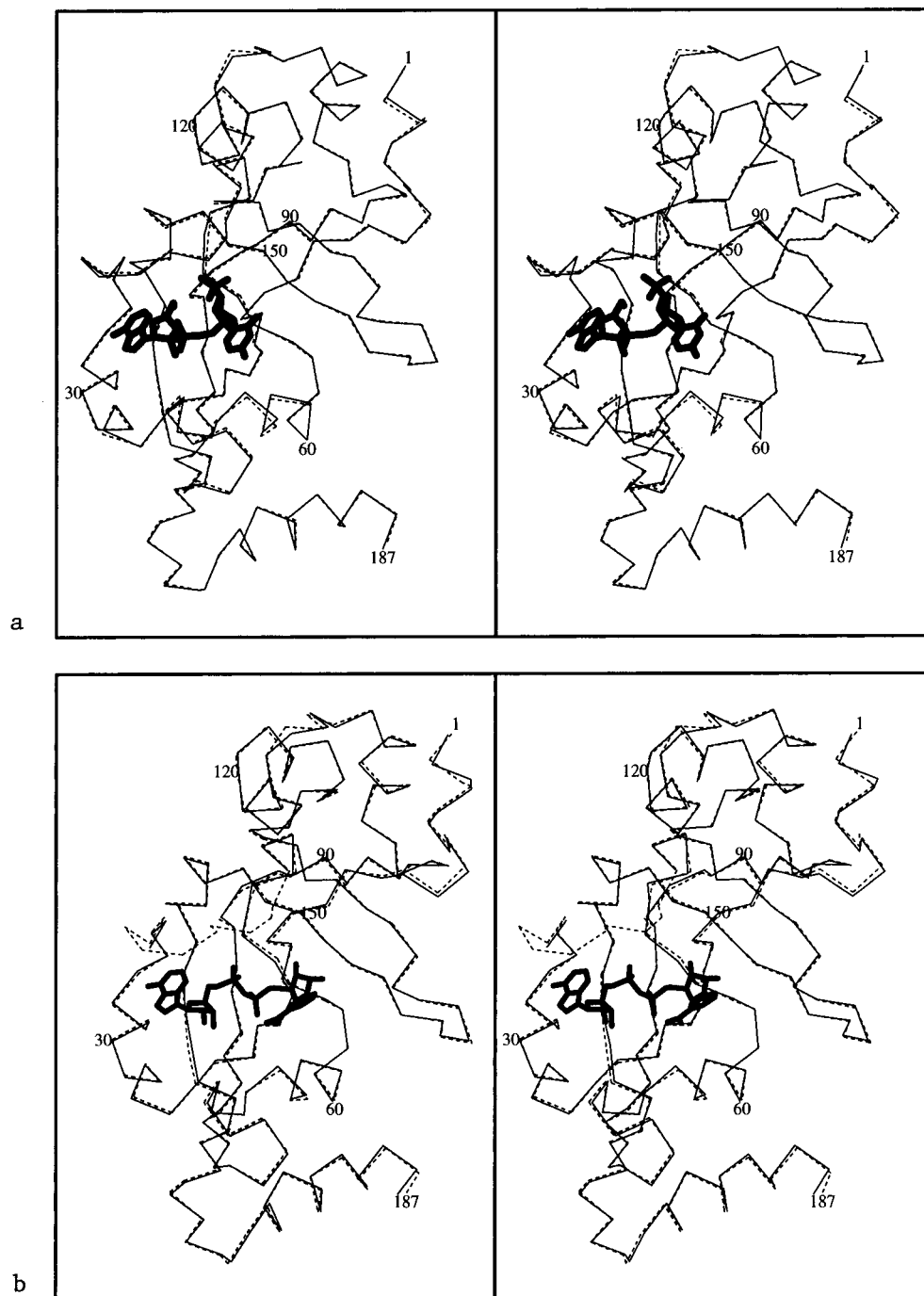
FIGURE 2: Stereoviews showing the structural alignment of the catalytic (C) domain of nucleotide-free DT with (a) DT bound to ApUp (PDB entry 1DDT; Bennett et al., 1994) and (b) DT bound to NAD (PDB entry 1TOX; Bell & Eisenberg, 1996). The Cα trace of nucleotide-free DT is shown in thin, dashed lines. The Cα traces of DT–ApUp and DT–NAD are shown in thin, solid lines. NAD and ApUp are shown in thick, solid lines. Notice that, except for residues 39–47 in dDT–NAD which are disordered (and thus are not shown), the binding of NAD and ApUp to the C domain does not affect the path of the protein backbone.

active-site cleft are observed, due to interactions with each of the dinucleotides. Figure 3 shows a closeup view of the active-site cleft in a structural alignment of the C domain of dDT-nf with dDT–ApUp (Figure 3a) and with dDT–NAD (Figure 3b). The most significant difference is in the position of the side chain of Tyr65. The phenyl ring of Tyr65 stacks against the uracil ring of ApUp and also the nicotinamide ring of NAD. In dDT-nf, the side chain of Tyr65 is positioned approximately 2.5 Å away from the active-site pocket, and rotated by ∼20°. Thus, upon nucleotide binding, the side chain of Tyr65 closes in by 2.5 Å to form tight stacking interactions. Similarly, Pro38, which forms part

of the hydrophobic adenine-binding pocket for both ApUp and NAD, is positioned ∼2 Å away from the active-site pocket in the structure of dDT-nf. Thus, upon ApUp or NAD binding, Pro38 moves ∼2 Å to pack against the adenine ring. Subtle movements are observed in the positions of Tyr27 and Tyr54. These residues also line the active-site cleft and interact with ApUp and NAD. In dDT-nf, these residues are positioned 0.5–1.0 Å away from the active-site cleft.

In a comparison of the dDT-nf and dDT–NAD structures, other significant differences are observed. In the dDT–NAD structure, the hydroxyl group of Thr23 moves by ∼3 Å, in
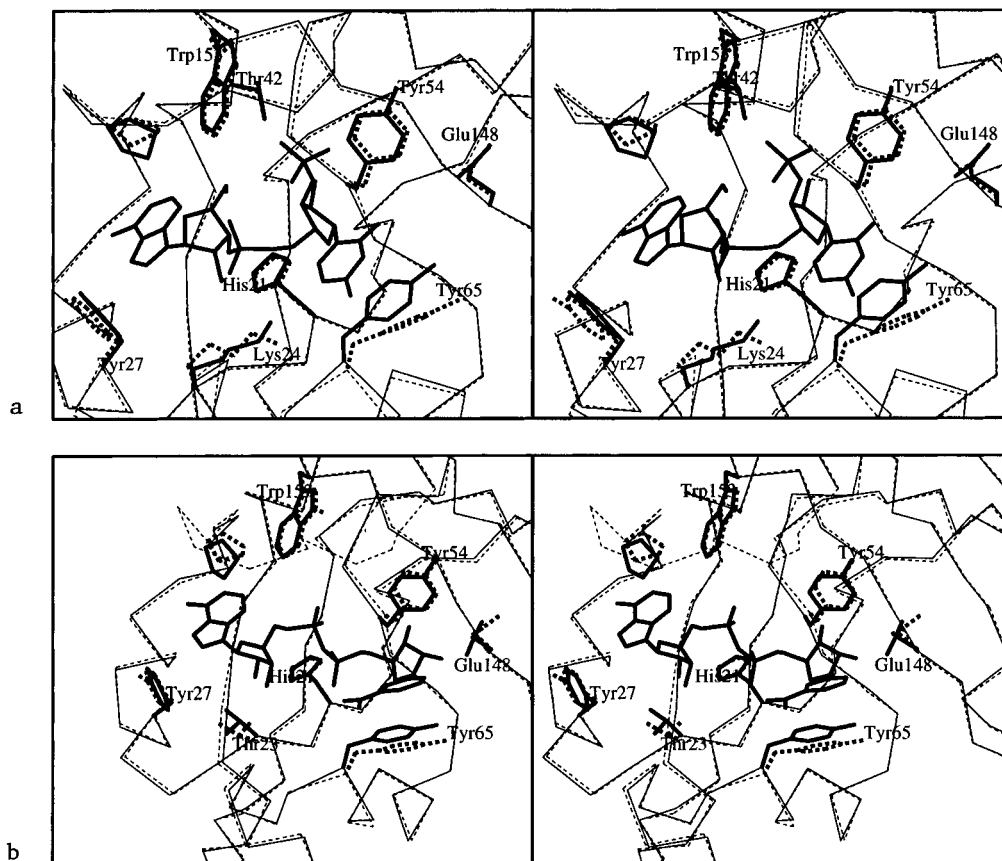
FIGURE 3: Closeup stereoview of the active-site cleft in an alignment of the structure of nucleotide-free DT with (a) DT bound to ApUp and (b) DT bound to NAD. As in Figure 2, the nucleotide-free DT structure is shown in dashed lines, while the DT−ApUp and DT−NAD structures are shown in solid lines. Notice that the side chains of Tyr65, Pro38, Tyr54, Tyr27, Thr23, and Glu148 show movements of up to 3 Å upon binding either NAD or ApUp.

order to hydrogen bond to the O2′ hydroxyl of the adenosine ribose of NAD. In addition, the caryboxylate group of Glu148 moves by ∼1.5 Å, in order to form a salt bridge with the positively charged N1 atom of the nicotinamide ring of NAD, and also to hydrogen bond to the O2′ hydroxyl of the nicotinamide ribose. In the dDT−ApUp structure, these interactions are not formed, and Thr23 and Glu148 are in the same position as in the dDT-nf structure.

The side chain of His21 is positioned identically in each of the three structures. While His21 hydrogen bonds to both NAD and ApUp, it also hydrogen bonds to the backbone carbonyl of Tyr54. The lack of movement of His21 is consistent with a role for this side chain in maintaining the structural integrity of the active-site cleft.

In summary, the structure of dDT-nf, as compared to dDT−NAD and dDT−ApUp, shows that upon nucleotide binding residues Tyr65 and Pro38 close in toward the active-site pocket to form hydrophobic or stacking interactions with the base rings of ApUp and NAD. Other movements are observed for the side chains of Thr23, Glu148, Tyr27, and Tyr54.

Active-Site Loop Conformation. In the dDT-nf crystal structure, residues 38−47 of the active-site loop are well ordered and extend over the active-site cleft in a conformation nearly identical to that in the dDT−ApUp structure. The electron density for these residues in the dDT-nf crystal structure is shown in Figure 4. The conformation of this loop over the active-site cleft is stabilized by several side chain to main chain hydrogen bonds, involving Pro38, Gln43,

Thr42, Tyr46, Asn45, Asp47, Asp48, Asp49, Lys51, Gly52, Tyr54, and Trp153. These interactions are shown in Figure 5.

However, in the structure of dDT−NAD, residues 39−47 of the active-site loop are disordered, for both of the DT-NAD complexes in the asymmetric unit of the dDT−NAD crystal. It appears that NAD binding somehow disrupts the interactions which stabilize the active-site loop, causing it to become disordered. Since the active-site loop of DT is apparently not involved in NAD binding, and since the sequence of this loop is similar in DT and ETA, which both catalyze the ADP ribosylation of EF-2, it was proposed that this loop may be important for binding to EF-2, the ADP ribose acceptor substrate of DT and ETA (Bell & Eisenberg, 1996). Thus, it is of interest to discern how NAD binding causes residues 39−47 of the active-site loop of DT to become disordered.

Figure 6 shows a superposition of the structure of dDT-nf and NAD from the structure of dDT−NAD. This superposition suggests that NAD does not directly displace the active-site loop through steric interactions, since the positions of the active-site loop and NAD do not directly overlap. The nearest point of contact between NAD and the active-site loop in the superposition is between the carbonyl oxygen of Gly44 and the O3′ NMN ribose hydroxyl, which are 3.3 Å apart. One possible explanation of how NAD binding disrupts the active-site loop structure is the movement of Pro38. The movement of the side chain of Pro38, driven by the formation of hydrophobic interactions
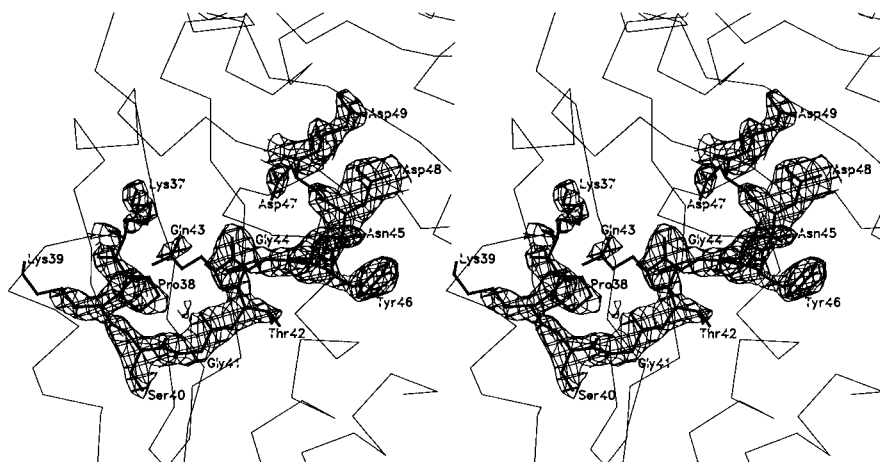
FIGURE 4: Stereoview of the electron density for the active-site loop in the crystal structure of nucleotide-free DT. A $2F_o - F_c$ annealed omit map (Hodel et al., 1992), contoured at 1σ, is shown in the region of residues Lys37−Asp49 of the active-site loop of DT. Notice that residues 39−47 of the active-site loop are well ordered, in contrast to being disordered in dDT−NAD (Bell & Eisenberg, 1996). This figure and Figures 5 and 6 were prepared using SETOR (Evans, 1993).
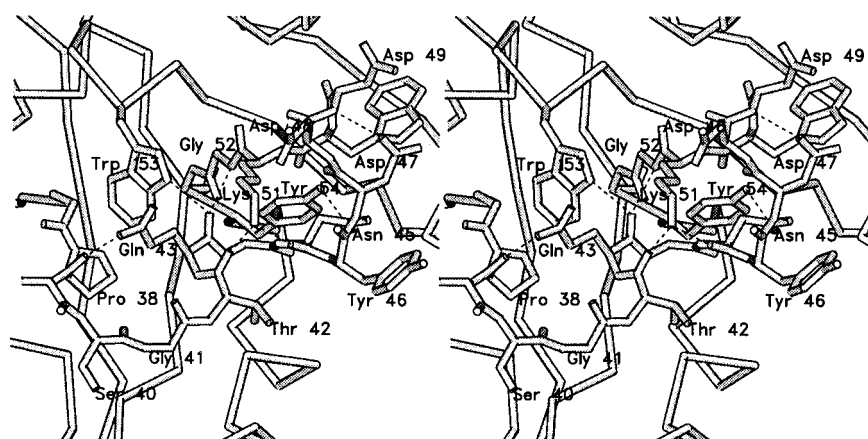

FIGURE 5: Stereoview showing the interactions which stabilize the conformation of the active-site loop in the structure of nucleotide-free DT. Hydrogen bonds are shown as thin dashed lines. Notice that the backbone carbonyl oxygen atom of Pro38 hydrogen bonds to the side chain of Gln43. The backbone carbonyl oxygen of Gln43 is in turn hydrogen-bonded to the side chain of Trp153 and the backbone amide of Gly52. These interactions form a network of main chain to side chain hydrogen bonds which stabilizes the position of the active-site loop over the active-site cleft in the structure of nucleotide-free DT.
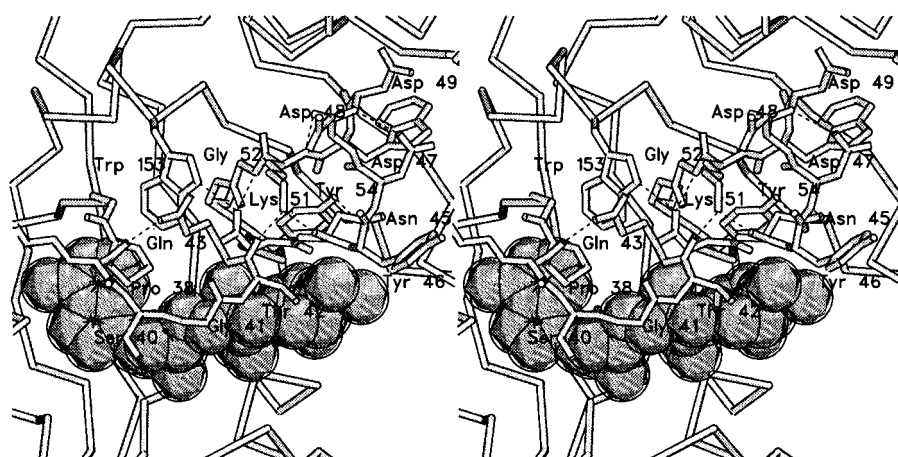

FIGURE 6: Stereoview showing a superposition of the active-site region of nucleotide-free DT and NAD from the DT−NAD crystal structure (PDB entry 1TOX; Bell & Eisenberg, 1996). NAD is shown in a space-filling representation. Notice that NAD does not directly superimpose with any residues of the active-site loop. Rather, subtle interactions with NAD, possibly involving Pro38, Tyr54, and Trp154, lead to the displacement of the active-site loop residues 39−47 from their position over the active-site cleft in dDT-nf to a disordered state in dDT−NAD.

with the adenine ring of NAD (see Figure 3b), could disrupt the hydrogen bond between the backbone carbonyl oxygen of Pro38 and the NE1 side chain atom of Gln43 (see Figures 5 and 6). This could in turn destabilize the network of hydrogen bonds that holds the active-site loop in place. In addition, the formation of interactions between NAD and

the side chains of Tyr54 and Trp153 could also disrupt the active-site loop structure, although these residues move only slightly upon NAD binding.

In summary, it appears that very subtle interactions between NAD and DT, possibly involving Pro38, Tyr54, and Trp153, release residues 39−47 of the active-site loop from their well-ordered position over the active-site cleft in dDT-nf. As discussed previously (Bell & Eisenberg, 1996), the NAD-binding-induced release of the active-site loop from the active-site cleft could be an important step in the subsequent binding of the ADP ribose acceptor substrate EF-2.

Comparison to Other ADP-Ribosylating Toxins. The atomic structures of five other ADP-ribosylating toxins have been determined by X-ray crystallography. These are ETA (Allured et al., 1986), LT-I (Sixma et al., 1993), LT-IIb (van den Akker et al., 1996), PT (Stein et al., 1994), and CT (Zhang et al., 1995). While the catalytic domains of DT and ETA ADP-ribosylate the diphthamide residue of EF-2, the catalytic domains of LT-I, LT-IIb, and CT ADP-ribosylate a particular arginine residue of the α-subunits of certain stimulatory heterotrimeric G-proteins, and the catalytic domain of PT ADP-ribosylates a particular cysteine residue of the α-subunits of certain inhibitory heterotrimeric G-proteins (Burnette et al., 1994). Despite a limited sequence identity of 10−20% among the catalytic domains of these toxins (except for LT-I, LT-IIb, and CT which share >60% sequence identity with one another), they all share a common core fold which forms the NAD-binding site. Intriguingly, the catalytic domain of each toxin possesses an active-site loop or segment, similar to the active-site loop of DT, that is positioned in or near the NAD-binding cleft. In each case, it appears that NAD binding is (or would necessarily be) accompanied by displacement of the active-site segment from the active-site cleft to either a disordered state or an alternative conformation.

In the structure of the catalytic domain of ETA, which is the most similar to the C domain of DT (∼20% sequence identity), residues 458−463 form an active-site loop that is topologically identical to the active-site loop of DT. The crystal structure of intact ETA, including domains I (receptor binding), II (translocation), and III (catalytic), has been determined in the absence of NAD (Allured et al., 1986). In addition, the isolated catalytic domain III of ETA, residues 400−613, has been determined in complex with an NAD analog (Li et al., 1996). In the nucleotide-free, intact ETA structure, active-site loop residues 458−463 of the catalytic domain are ordered and positioned right over the NAD-binding cleft (Figure 7a). Although this particular conformation of the active-site loop may be affected by contacts with residues 341−348 of domain II of ETA, there are five hydrogen bonds involving residues 458−468 of the catalytic domain of ETA which also stabilize the conformation of the active-site loop observed in intact ETA.

In the structure of the isolated catalytic domain of ETA complexed with an NAD analog (Li et al., 1996), there are two independent molecules in the asymmetric unit of the crystal. In molecule 1, the active-site loop residues 458−463 are disordered (Figure 7b). In molecule 2, these residues are ordered but in a conformation different from that observed in the nucleotide-free, intact ETA structure, apparently due to contacts with a symmetry-related molecule in the crystal (Li et al., 1996). Interestingly, the NAD-
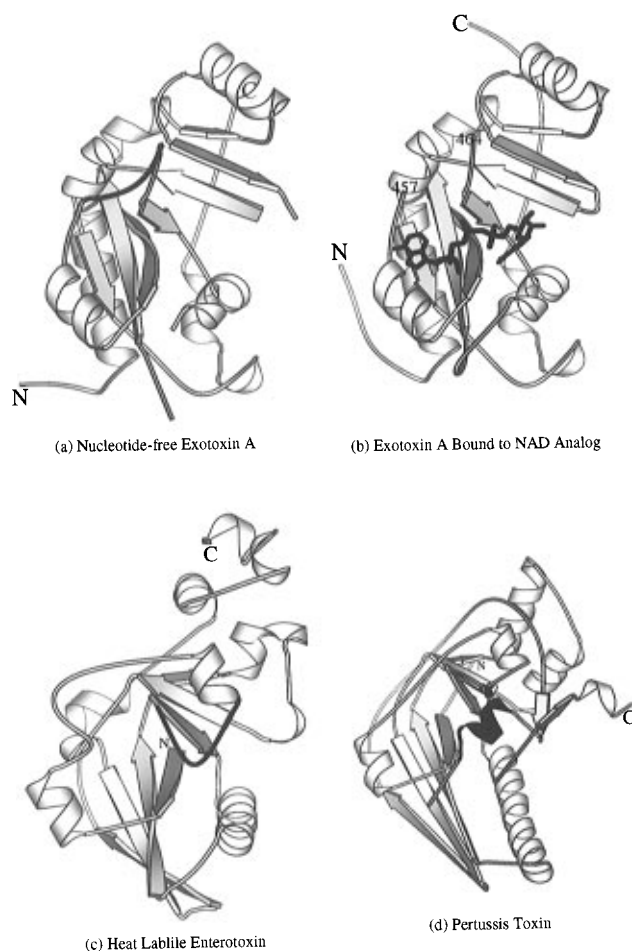
FIGURE 7: Active-site loops of the catalytic domains of the ADP-ribosylating toxins. Notice that the catalytic domains of the ADP-ribosylating toxins share a common core fold formed by two approximately orthogonal antiparallel β-sheets. The NAD-binding site is at the interface between the two β-sheets. (a) Structure of the catalytic domain of ETA from the crystal structure of intact ETA (domains I and II are not shown), with coordinates kindly provided by David McKay (Allured et al., 1986). Residues 458−463 of the active-site loop of ETA, which are highlighted in black, are positioned over the NAD-binding site. (b) Structure of the isolated catalytic domain of ETA complexed with an NAD analog (Li et al., 1996; PDB entry 1AER) for molecule 1 of the asymmetric unit of the crystal. Residues 458−463 of the active-site loop of ETA are disordered and are not shown; residues 457 and 464 are labeled. For the second independent molecule of the catalytic domain of ETA bound to the NAD analog, residues 458−463 are ordered but are stabilized by contacts with a symmetry-related molecule (not shown). (c) Structure of the catalytic domain of LT-I (Sixma et al., 1991; PDB entry 1LTS). Residues 47−56 of LT, which are shown in black, form a loop that is positioned in the presumed NAD-binding site and would therefore most probably be displaced upon NAD binding. The catalytic domains of LT-IIb (van den Akker et al., 1995) and CT (Zhang et al., 1995) are >60% identical in sequence to LT-I and have nearly identical active-site loop structures. (d) Stucture of the catalytic S1 subunit of PT (Stein et al., 1994; PDB entry 1PRT). Residues 199−207 of PT, which are highlighted in black, form a helix that is positioned in the presumed NAD-binding site and would therefore most probably be displaced upon NAD binding.

binding site observed in the structure of the catalytic domain of ETA bound to the NAD analog overlaps with residues Arg458 and Gln460 of the active-site loop as seen in the intact, nucleotide-free ETA structure. This suggests that NAD binding to domain III of ETA may displace the active-site loop residues 458−463 of ETA. This would be similar to the displacement of residues 38−46 of the catalytic domain

of DT upon NAD binding. Although crystals of the isolated catalytic domain of ETA could not be grown in the absence of the NAD analog, when these crystals were soaked in mother liquor lacking the NAD analog, the density for the NAD analog disappeared, but active-site loop residues 458−463 of ETA remained disordered. This suggests that the active-site loop of ETA may not be ordered in the absence of NAD (Li et al., 1996). In any case, the active-site loop of ETA, like that of DT, exhibits conformational flexibility in the presence of NAD.

In the structure of the catalytic domain of LT-I (as well as the catalytic domains of LT-IIb and CT which are 63 and 80% identical to LT-I, respectively), there is an active-site loop, residues 47−56, that is topologically similar to the active-site loops of DT and ETA (Figure 7c). Although the structure of LT-1 in complex with NAD has not been determined, in the nucleotide-free structure of LT-I, this loop is positioned in the active-site cleft, overlapping with the presumed NAD-binding site (Sixma et al., 1993). Thus, in order for NAD to bind, the active-site loop of LT-I must be displaced from its position in the active-site cleft to either a disordered state or an alternative conformation. Indeed, in the crystal structure of an Arg7Lys mutant of LT-I, residues 47−56 of the active-site loop were found to be disordered, demonstrating the potential this loop has for flexibility (van den Akker et al., 1995). Mutation of Val53 of the active-site loop of LT to Asp diminishes the ADP ribosylation activity, suggesting that this loop may have an essential activity (Pizza et al., 1994). By analogy with the active-site loop of DT, this loop of LT could be important for binding to the heterotrimeric G-proteins which are the ADP ribose acceptor substrates for LT.

The catalytic domain of PT, called the S1 subunit, does not have an active-site loop which is topologically similar to those of DT, ETA, and LT. However, residues 199−207 near the C terminus of S1 form a short helix that is positioned in the active-site cleft (Figure 7d), overlapping with the presumed NAD-binding site (Stein et al., 1994). Cys201 of this helix forms a disulfide bond with Cys41 within the active-site cleft, the reduction of which is required for activity. Thus, although the NAD-bound structure of PT has not been determined, it is likely that NAD binding to the active site of S1 would be accompanied by displacement of residues 199−207 from their position in the active-site cleft to either an alternative conformation or a disordered state. Deletion mutagenesis studies have shown that residues 195−219 of S1 (including active-site helix residues 199−207) are required for full ADP ribosylation activity but not for NAD glycohydrolase activity. It was therefore concluded that this stretch of residues is likely to function in binding to the heterotrimeric G-proteins which are the ADP ribose acceptor substrates for the S1 subunit of PT (Cortina et al., 1991).

In summary, it appears that the feature of an active-site loop or helical segment that is positioned in or near the NAD-binding site, and is displaced upon NAD binding, is conserved for the group of ADP-ribosylating toxins whose structures have been determined by X-ray crystallography. In the case of PT, mutational studies have provided evidence that this segment is important for binding to the heterotrimeric G-protein ADP ribose acceptor substrate. For DT, ETA, and LT, such mutational data addressing the possible functions of the active-site loops are at present lacking. However, for DT and ETA, it seems clear from crystal structures of the NAD complexes that the active-site loops are not important for NAD binding and thus could likely function in binding to EF-2, the ADP ribose acceptor substrate.

REFERENCES

Allured, V. S., Collier, R. J., Carroll, S. F., & Mckay, D. B. (1986) *Proc. Natl. Acad. Sci. U.S.A. 83*, 1320−1324.

Bell, C. E., & Eisenberg, D. (1996) *Biochemistry 35*, 1137−1149.

Bennett, M. J., & Eisenberg, D. (1994) *Protein Sci. 3*, 1464−1475.

Bennett, M. J., Choe, S., & Eisenberg, D. (1994) *Protein Sci. 3*, 1444−1463.

Brünger, A. T. (1990) *X-PLOR Manual*, Version 3.1, Yale University, New Haven, CT.

Burnette, W. N. (1994) *Structure 2*, 151−158.

Carroll, S. F., Barbieri, J. T., & Collier, R. J. (1986) *Methods Enzymol. 165*, 68−76.

Choe, S., Bennett, M. J., Fujii, G., Curmi, P. M. G., Kantardjieff, K. A., Collier, R. J., & Eisenberg, D. (1992) *Nature 357*, 216−222.

Collier, R. J. (1975) *Bacteriol. Rev. 39*, 54−85.

Cortina, G., Krueger, K. M., & Barbieri, J. T. (1991) *J. Biol. Chem. 266* (35), 23810−23814.

Evans, S. V. (1993) *J. Mol. Graphics 1*, 134−138.

Freeman, V. J. (1951) *J. Bacteriol. 61*, 675−88.

Fujii, G., Choe, S., Bennett, M. J., & Eisenberg, D. (1991) *J. Mol. Biol. 222*, 861−864.

Greenfield, L., Bjorn, M. J., Horn, D., Fong, D., Buck, G. A., Collier, R. J., & Kaplan, D. A. (1983) *Proc. Natl. Acad. Sci. U.S.A. 80*, 6853−6857.

Hodel, A., Kim, S. H., & Brünger, A. T. (1992) *Acta Crystallogr. A48*, 851−858.

Kabsch, W. (1978) *Acta Crystallogr. A34*, 827−828.

Kraulis, P. J. (1991) *J. Appl. Crystallogr. 24*, 946−950.

Li, M., Dyda, F., Benhar, I., Pastan, I., & Davies, D. R. (1996) *Proc. Natl. Acad. Sci. U.S.A. 93*, 6902−6906.

Moss, J., & Vaughn, M. (1990) in *ADP-Ribosylating toxins and G proteins: Insights into signal transduction*, American Society for Microbiology, Washington, DC.

Pappenheimer, A. M., Jr. (1977) *Annu. Rev. Biochem. 46*, 69−94.

Passador, L., & Iglewski, W. (1994) *Methods Enzymol. 235*, 617−630.

Pizza, M., Domenighini, M., Hol, W., Gianelli, V., Fontana, M. R., Giuliani, M. M., Magagnoli, C., Peppoloni, S., Manetti, R., & Rappuoli, R. (1994) *Mol. Microbiol. 14* (1), 51−60.

Ruf, A., De Murcia, J. M., De Murcia, G. M., & Schulz, G. E. (1996) *Proc. Natl. Acad. Sci. U.S.A. 93*, 7481−7485.

Sixma, T. K., Kalk, K. H., van Zanten, B. A. B., Dauter, Z., Kingma, J., Witholt, B., & Hol, W. G. J. (1991) *Nature 355*, 561−564.

Stein, P. E., Boodhoo, A., Armstrong, G. D., Cockle, S. A., Klein, M. H., & Read, R. J. (1994) *Structure 2*, 45−47.

Takada, T., Iida, K., & Moss, J. (1995) *J. Biol. Chem. 270*, 541−544.

van den Akker, F., Merritt, E. A., Pizza, M. G., Domenighini, M., Rappuoli, R., & Hol, W. G. J. (1995) *Biochemistry 34*, 10996−11004.

van den Akker, F., Sarfaty, S., Twiddy, E. M., Connell, T. D., Holmes, R. K., & Hol, W. G. J. (1996) *Structure 4*, 665−678.

van Ness, B. G., Howard, J. B., & Bodley, J. W. (1980) *J. Biol. Chem. 255*, 10710−10716.

Weiss, M. S., Blanke, S. R., Collier, R. J., & Eisenberg, D. (1995) *Biochemistry 34*, 773−781.

Zhang, R.-G., Scott, D. L., Westbrook, M. L., Nance, S., Spangler, B. D., Shipley, G. G., & Westbrook, E. M. (1995) *J. Mol. Biol. 251*, 563−573.

BI962214S